

# Dynamic response of metamaterials in the terahertz regime: Blueshift tunability and broadband phase modulation

J.-M. Manceau,<sup>1</sup> N.-H. Shen,<sup>1</sup> M. Kafesaki,<sup>1,2</sup> C. M. Soukoulis,<sup>1,2,3</sup> and S. Tzortzakis<sup>1,a)</sup>

<sup>1</sup>Institute of Electronic Structure and Laser (IESL), Foundation for Research and Technology–Hellas (FORTH), P.O. Box 1527, 71110 Heraklion, Greece

<sup>2</sup>Department of Materials Science and Technology, University of Crete, 71003 Heraklion, Greece

<sup>3</sup>Department of Physics and Astronomy and Ames Laboratory, Iowa State University, Ames, Iowa 50011, USA

(Received 2 September 2009; accepted 22 December 2009; published online 15 January 2010)

Terahertz time-domain spectroscopy is used to probe the electromagnetic properties of metamaterials, which are dynamically photoexcited, using synchronized femtosecond near-infrared laser pulses. Blueshift tunability of the electric dipole metamaterial's resonance, as well as a broadband phase tunability reaching  $\sim\pi/4$ , are demonstrated. Numerical simulations show the observations are due to changes in the complex index of the photoexcited semiconductor substrate. © 2010 American Institute of Physics. [doi:10.1063/1.3292208]

Research on metamaterials, i.e., artificially structured subwavelength materials, in recent years has grown exponentially. The main reason behind this interest is the peculiar electromagnetic response of these metamaterials not available in naturally occurring media.<sup>1</sup> Fundamental and applied research on metamaterials, spanning from radio frequencies to optical wavelengths,<sup>2</sup> have demonstrated a variety of interesting phenomena, such as negative refraction,<sup>3</sup> subdiffraction-limited imaging,<sup>4</sup> and electromagnetic cloaking.<sup>5</sup>

More recently, considerable advances have been made on research related to terahertz (THz) metamaterials and have led to the development of various metamaterial components to control the THz radiation properties. Components, such as frequency tunable filters,<sup>6,7</sup> all-optical switches and modulators,<sup>7-9</sup> and perfect absorbers,<sup>10</sup> have already been demonstrated experimentally. Recently, Chen *et al.*<sup>11</sup> demonstrated efficient phase shifting devices in the THz range. A single layer planar hybrid metamaterial made of split-ring resonators (SRRs) on top of a highly doped semiconductor layer was used. Applying external voltage to the structure, a direct control of the carrier density in the depletion zone of the metal-semiconductor interface was demonstrated, which, in turn, directly tuned the dielectric properties near the gaps of the SRRs, leading to a phase change over a narrow band of frequency (23 GHz). Also, specifically designed metamaterial structures have been proposed for THz polarimetric devices.<sup>12</sup>

In this letter, we report on the ability to obtain tunable electric resonance responses in the THz regime, as well as a broadband ( $\sim 250$  GHz) phase tunability (over  $\sim\pi/4$ ), using classical metamaterials consisting of metallic SRRs on the top of a semiconductor substrate. The tunability is achieved dynamically by photoexciting the metamaterial, using intense near-infrared femtosecond laser pulses. Numerical calculations, using a simple Drude model, can explain the experimental observations, as a result of the changes induced on the complex index of refraction of the photoexcited semiconductor substrate.

The metamaterial sample under study is the same as the one studied in Ref. 8, i.e., it consists of an array of SRRs, fabricated from copper, deposited on 670  $\mu\text{m}$  thick, high resistivity GaAs substrate. A sketch of the experimental approach, together with the exact dimensions of the SRRs, is given in Fig. 1.

The experimental study of this system was performed using THz time domain spectroscopy (TDS). For this experiment, a powerful THz-TDS system has been developed, using an amplified kHz Ti:Sa laser system delivering 35 fs pulses at 800 nm central wavelength and maximum energy equal to 1.3 mJ was focused in ambient air after partial frequency doubling in a beta-barium-borate crystal (50  $\mu\text{m}$  thick) to produce a two-color filament and subsequently, THz radiation.<sup>13</sup>

Ultrashort laser pulse filamentation is a well-known phenomenon of laser beam self-organization in a narrow intense filamentary structure, which results from competition between linear and nonlinear effects, including the Kerr self-focusing, ionization defocusing, nonlinear losses, and dispersion effects.<sup>14</sup> Inside the filament, the presence of the second harmonic field, slightly out of phase from the fundamental,

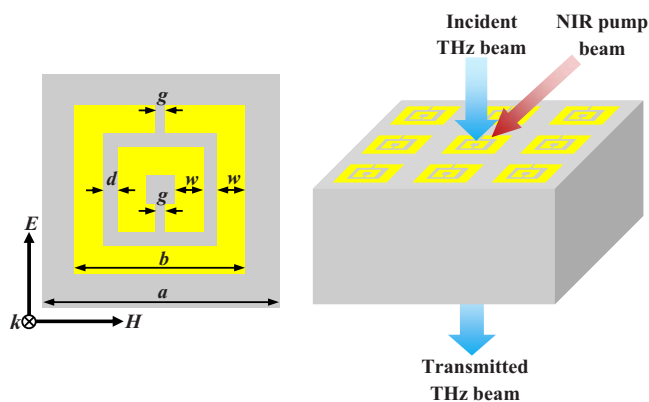


FIG. 1. (Color online) The SRR design studied. The vectors show the incident THz electromagnetic field orientation for the case of parallel orientation (to the gap). The geometrical parameters of the system are as follows:  $a = 50 \mu\text{m}$ ,  $b = 36 \mu\text{m}$ ,  $d = 3 \mu\text{m}$ ,  $g = 2 \mu\text{m}$ , and  $w = 6 \mu\text{m}$ .

<sup>a)</sup>Electronic mail: stzortz@iesl.forth.gr.

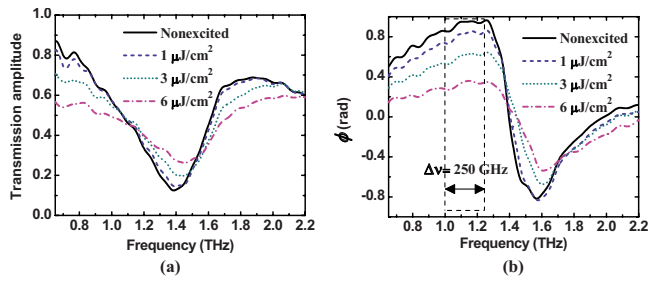


FIG. 2. (Color online) Experimental transmission amplitude spectra (a) and phase tunability (b) for different levels of photoexcitation.

produces an asymmetry in the ionizing field. Consequently, a net ionization current is formed, leading to forward emission of THz pulses.<sup>13,15,16</sup>

For the detection of THz radiation, a small fraction of the initial laser pulse probed the THz-induced birefringence in an electro-optic crystal (ZnTe 1 mm thick) and monitored the time profile of the THz electric field.<sup>17</sup> The entire experimental setup was placed inside a purge gas chamber to avoid water vapor absorption of the THz radiation.

To study the dynamic response of the metamaterial, an optical-pump beam was used to excite photocarriers in the GaAs substrate. The sample was placed orthogonally on the THz beam path and at the focus of the THz beam (see Fig. 1). At this point the THz beam spot's diameter measured about 1.2 mm. The optical pump was launched at 45° on the sample. The temporal synchronization of the THz and the optical pump beams have been experimentally defined. Afterwards, the THz pulse was delayed to assure a 5 ps average (because of the angle between the two beams) delay between them. This 5 ps delay was used to assure a quasisteady state of the injected photocarriers, since they have a lifetime in the nanoseconds regime.

The theoretical study of our metamaterial system was performed using the finite-integration technique, employed through the well-established commercial software CST MICROWAVE STUDIO. The simulations were performed by considering one unit cell of the system embedded in a waveguide with electric and magnetic boundaries to support a constant profile transverse electromagnetic wave. Waveguide ports were used as source and detector to monitor the transmission and reflection properties of this system. In the simulations, the substrate refractive index (for the nonphotoexcited substrate) was taken as 12.7, and the copper conductivity  $5.8 \times 10^7$  S/m.

To validate our theoretical and experimental procedures, we repeated the study presented in Ref. 8. Two resonances were observed in the case of perpendicular polarization (not shown here) and a single broad resonance for the case of parallel polarization [see Fig. 2(a)]. The dynamical study of the SRR with its gap perpendicularly orientated to the THz electric field has also been conducted. The results reported in Ref. 8 were reproduced.

In this letter, though our effort is turned toward the behavior of the parallel orientation electric resonance under photoexcitation, which has not been investigated previously. For different levels of excitation fluence, the THz electric field was recorded. The results are shown in Fig. 2(a). The first observation from Fig. 2(a) is the presence of an amplitude modulation of the resonance when photocarriers are excited. This broad resonance is the dipolelike resonance of the

structure, related to the finite length of the metallic element along the electric field direction; thus, its amplitude modulation cannot be related to the short-circuit phenomenon observed for the magnetic resonance frequency shown in Ref. 8. Instead, this phenomenon should be related to the change in conductivity of the substrate, where increasing amounts of charges finally screens the existing resonance.

More interestingly, it is also possible to observe a frequency shift toward higher values (up to 50 GHz) as photocarriers are injected within the substrate [see Fig. 2(b)]. Such a shift was also observed in Ref. 8 for the case of perpendicular orientation, but its origin was not addressed. As electrons and holes are created under photoexcitation within the substrate (over one penetration depth; 1  $\mu\text{m}$  at 800 nm), the complex index of refraction is expected to change as well and can explain the experimental observations, except from changes in the conductivity.

Before moving to the theoretical analysis, let us consider the phase information from the experimental data. By determining the ratio between the extracted phase with and without photoinjection of carriers, one can characterize the phase shift,  $\Delta\phi$ , produced by the photoexcitation of the sample. Figure 2(b) clearly shows an almost flat phase shift extending over a very broad range of frequencies (from 1 to 1.25 THz), just before the anomalous phase shift on the resonance. The phase shift amplitude decreases as the photoexcitation becomes more important, forming practically a tunable THz wave plate. Although the losses are not negligible, this is still a remarkable result, considering this level of phase shift is achieved over a very broad spectral range and for a neither specifically designed nor optimized metamaterial.

To understand the origin of the frequency and phase tunability, we first conducted a series of simulations considering only the effect of a conductivity change. In this condition, only a redshift of the resonant frequency was observed. The blueshift of the resonance frequency would most probably be due to photoexcitation-induced dynamic response of the GaAs substrate beneath the SRRs. To fit the experimental results, we used the well-known Drude model, capable of describing the dynamic behavior of GaAs accurately within our considered frequency regime.<sup>18,19</sup> We first assume the photoexcited layer with a thickness (i.e., penetration depth),  $d$ , of a typical value, 1  $\mu\text{m}$ . The frequency-dependent complex conductivity takes the form  $\sigma = \epsilon_0 \omega_p^2 / (\gamma - i\omega)$ , where  $\epsilon_0$  is the permittivity of vacuum,  $\gamma$  represents the collision frequency, and  $\omega_p = \sqrt{Ne^2 / (\epsilon_0 m^*)}$  the plasma frequency.  $N$  is the carrier density,  $e$  is the free electron charge ( $1.6 \times 10^{-19}$  C), and  $m^* = 0.067m_0$  ( $m_0$  is the mass of the free electron), the effective carrier mass in  $n$ -doped GaAs. Then, the dielectric constant  $\epsilon(\omega)$  is obtained, based on  $\sigma(\omega)$  by  $\epsilon(\omega) = \epsilon_s + i\sigma / (\epsilon_0 \omega)$ , where  $\epsilon_s$  is the dielectric constant of undoped GaAs.

To fit the resonance frequency at 1.4 THz for the case of a nonilluminated sample, we used  $\epsilon_s = 12.7$ , and we kept this value throughout our fitting procedure for all cases. Next, we focused on the photodoping cases. According to the Drude model, it is easily found that the carrier density,  $N$ , and collision frequency,  $\gamma$ , are pending quantities, which together determine the properties of the photoexcited layer and the response of the sample. In our fitting procedure,  $\gamma$  should be kept constant for any set of  $N$  because the mobility of the

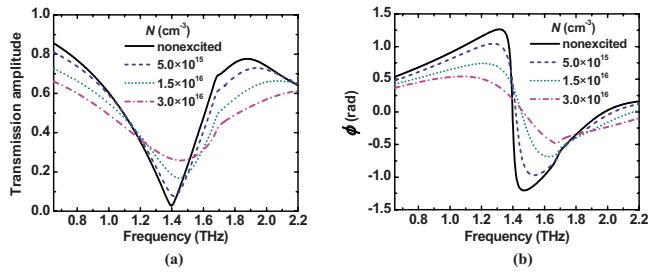


FIG. 3. (Color online) Simulation results of the transmission amplitude spectra (a) and phase modulation (b) for different levels of carrier density  $N$ .

carriers changes slightly within the explored carrier density range. By fitting the resonance frequencies and corresponding transmission amplitudes, and simultaneously considering the transmission levels at a low frequency band, the collision frequency,  $\gamma$ , is taken as 1.8 THz and the retrieved values of the carrier density  $N$  are  $3 \times 10^{16}$ ,  $1.5 \times 10^{16}$ , and  $5 \times 10^{15} \text{ cm}^{-3}$  for the excitation at 6, 3, and  $1 \mu\text{J}/\text{cm}^2$ , respectively. The simulated results of the transmission spectra fit well with the experimental ones, as shown in Fig. 3(a).

In the simulations, we also extracted the phase information of the transmission for the different cases. These results are presented in Fig. 3(b). Similar to the experimental results, we also can observe the interesting phase modulation effect almost as impressive as in the experiments.

In conclusion, we have shown the existence of a frequency shift under injection of photocarriers related to the change in the refractive index of the GaAs substrate. Also, an important phase tunability (over  $\sim \pi/4$ ) for a large frequency bandwidth ( $\sim 250 \text{ GHz}$ ) was observed, which demonstrates the possibility of phase modulation under photoexcitation, consequently, opening the way to the realization of simple broadband phase plate devices in the THz range.

We would like to thank Willie J. Padilla for providing us the sample and Lei Zhang for her kind help with simulations. This work was supported by the European Union Marie

Curie Excellence Grant “MULTIRAD” under Grant No. MEXT-CT-2006-042683. This work was also partially supported by the European Community projects, PHOME (FET Contract No. 213390), ENSEMBLE (NMP-STREP) and ECONAM (NMP-CA), the cost actions MP0702 and MP0803, and the Air Force Material Command USAF (Grant No. FA8655-07-1-3037). Work at Ames Laboratory was supported by the Department of Energy (Basic Energy Sciences) under Contract No. DE-AC02-00-07CH11358.

- <sup>1</sup>D. R. Smith, J. B. Pendry, and M. C. K. Wiltshire, *Science* **305**, 788 (2004).
- <sup>2</sup>C. M. Soukoulis, S. Linden, and M. Wegener, *Science* **315**, 47 (2007).
- <sup>3</sup>R. A. Shelby, D. R. Smith, and S. Schultz, *Science* **292**, 77 (2001).
- <sup>4</sup>N. Fang, H. Lee, C. Sun, and X. Zhang, *Science* **308**, 534 (2005).
- <sup>5</sup>D. Schurig, J. J. Mock, B. J. Justice, S. A. Cummer, J. B. Pendry, A. F. Starr, and D. R. Smith, *Science* **314**, 977 (2006).
- <sup>6</sup>H. T. Chen, J. F. O’Hara, A. K. Azad, A. J. Taylor, R. D. Averitt, D. B. Shrekenhamer, and W. J. Padilla, *Nat. Photonics* **2**, 295 (2008).
- <sup>7</sup>N. H. Shen, M. Kafesaki, Th. Koschny, L. Zhang, E. N. Economou, and C. M. Soukoulis, *Phys. Rev. B* **79**, 161102(R) (2009).
- <sup>8</sup>W. J. Padilla, A. J. Taylor, C. Highstrete, M. Lee, and R. D. Averitt, *Phys. Rev. Lett.* **96**, 107401 (2006).
- <sup>9</sup>H. T. Chen, W. J. Padilla, J. M. O. Zide, S. R. Bank, A. C. Gossard, A. J. Taylor, and R. D. Averitt, *Opt. Lett.* **32**, 1620 (2007).
- <sup>10</sup>N. I. Landy, S. Sajuyigbe, J. J. Mock, D. R. Smith, and W. J. Padilla, *Phys. Rev. Lett.* **100**, 207402 (2008).
- <sup>11</sup>H. T. Chen, W. J. Padilla, M. J. Cich, A. K. Azad, R. D. Averitt, and A. J. Taylor, *Nat. Photonics* **3**, 148 (2009).
- <sup>12</sup>X. G. Peralta, E. I. Smirnova, A. K. Azad, H. T. Chen, A. J. Taylor, I. Brener, and J. F. O’Hara, *Opt. Express* **17**, 773 (2009).
- <sup>13</sup>K. Y. Kim, A. J. Taylor, J. H. Glowina, and G. Rodriguez, *Nat. Photonics* **2**, 605 (2008).
- <sup>14</sup>A. Couairon and A. Mysyrowicz, *Phys. Rep.* **441**, 47 (2007).
- <sup>15</sup>M. Chen, A. Pukhov, X. Y. Peng, and O. Willi, *Phys. Rev. E* **78**, 046406 (2008).
- <sup>16</sup>V. B. Gildenburg and N. V. Vvedenskii, *Phys. Rev. Lett.* **98**, 245002 (2007).
- <sup>17</sup>G. Gallot and D. Grischkowsky, *J. Opt. Soc. Am. B* **16**, 1204 (1999).
- <sup>18</sup>N. Katzenellenbogen and D. Grischkowsky, *Appl. Phys. Lett.* **61**, 840 (1992).
- <sup>19</sup>M. C. Beard, G. M. Turner, and C. A. Schmuttenmaer, *Phys. Rev. B* **62**, 15764 (2000).